Angewandte Chemie
Eine Zeitschrift der Gesellschaft Deutscher Chemiker

Supporting Information

Reduction of π-Expanded Cyclooctatetraene with Lithium: Stabilization of the Tetra-Anion through Internal Li^+ Coordination

Zheng Zhou, Yikun Zhu, Zheng Wei, John Bergner, Christian Neiß, Susanne Doloczki, Andreas Görling, Milan Kivala, and Marina A. Petrukhina**

anie_202013353_sm_miscellaneous_information.pdf

Table of Contents

1 Instrumentation and Materials

General. All reactions involving oxygen- or moisture-sensitive compounds were carried out in a dry reaction vessel under an inert atmosphere of nitrogen or argon using anhydrous solvents and standard Schlenk techniques unless otherwise noted. Dry solvents were obtained from an M. Braun MB SPS-800 solvent purification system or purchased from Fisher Scientific. All oxygen- and moisture-sensitive liquids and anhydrous solvents were transferred via a syringe or a stainless-steel cannula. Reaction mixtures were deoxygenated via a constant flow of nitrogen through the solution for 10 min. Photochemical reactions were carried out in a custom-built photoreactor system (Peschl Ultraviolet) using a water-cooled medium-pressure lamp (Peschl Ultraviolet, TQ51-HG and TQ150, 150 W, λ = 300–600 nm) in a quartz glass tube. Analytical thin-layer chromatography (TLC) analysis was performed on aluminum plates coated with 0.20 mm silica gel containing a fluorescent indicator (Macherey-Nagel, ALUGRAM®, SIL G/UV_{254}) or on aluminum plates coated with 0.20 mm Al_2O_3 containing a fluorescent indicator (Macherey-Nagel, ALUGRAM®, Alox N/UV_{254}). TLC plates were visualized by exposure to ultraviolet light (λ = 254 nm and 366 nm). Column chromatography was performed on silica gel (Macherey-Nagel, M-N Silica Gel 60A, 230–400 mesh) or Al_2O_3 (Macherey-Nagel, aluminum oxide 90 neutral or basic, 50–200 µm).

Solvents and Reagents. Reagents were purchased at reagent grade from common commercial sources (SIGMA-ALDRICH, Fisher Scientific, and abcr) and used without further purification. THF and toluene were used from a solvent purifying system (Braun SPS 800). Deuterated solvents were obtained from Deutero GmbH, Armar, and SIGMA-ALDRICH. $MgSO_4$ and Na_2SO_4 were used as drying agents after aqueous workup.

Reduction Reactions. All manipulations were carried out using break-and-seal[1] and glove-box techniques under an atmosphere of argon. Tetrahydrofuran (THF, Sigma Aldrich) and hexanes (Sigma Aldrich) were dried over Na/benzophenone and distilled prior to use. THF-d_8 (Sigma Aldrich) was dried over NaK_2 alloy and vacuum-transferred. Lithium metal (Sigma Aldrich, 99%) was used as received.

Instrumentation. ^{1}H and ^{13}C NMR spectra were recorded on a Bruker Avance 300 (Bruker, 300 MHz for ^{1}H, and 75 MHz for ^{13}C), a Bruker Avance 400 (Bruker, 400 MHz for ^{1}H and 101 MHz for ^{13}C), a Bruker Avance 500 (Bruker, 500 MHz for ^{1}H and 126 MHz for ^{13}C), and a

Bruker Avance 600 (Bruker, 600 MHz for ^{1}H, 151 MHz for ^{13}C) spectrometer. Chemical shifts (δ) are reported in parts per million (ppm) and are referenced to the residual solvent signal as an internal reference ($CDCl_3$: 7.26 ppm for ^{1}H, 77.16 ppm for ^{13}C). Coupling constants (J) are given in Hz and the apparent resonance multiplicity is reported as s (singlet), d (doublet), dd (doublet of doublet), dt (doublet of triplet), ddd (doublet of doublet of doublets), t (triplet), td (triplet of doublet), q (quartet), quint (quintet) or m (multiplet). All ^{13}C NMR spectra were generally recorded ^{1}H-decoupled ($\{^{1}H\}$). $CDCl_3$ (Deutero GmbH, 99.8%) were dried over molecular sieves (4 Å) prior to use. All spectra were recorded at ambient probe temperature, if not otherwise stated.

Mass spectra were obtained from an ApexQe hybrid 9.4 T FT-ICR (Bruker, ESI, MALDI, DART) or an AutoFlex Speed TOF (Bruker, LDI, MALDI) (Institute of Organic Chemistry, Heidelberg University).

Melting points (mp) were determined on a Büchi M-560 melting point apparatus in open capillaries. “Decomp.” refers to decomposition.

The ^{1}H NMR and ^{7}Li NMR spectra for $[\{Li^{+}(THF)_4\}_2\{Li^{+}{}_2(1^{4-})\}]$ (**2**) were recorded on a Bruker Ascend-500 spectrometer (Bruker, 500 MHz for ^{1}H and 194.317 MHz for ^{7}Li). Chemical shifts (*δ*) are reported in parts per million (ppm) and referenced to the resonances of the corresponding solvent used. The low-temperature NMR experiment was controlled by a Cryo Diffusion cryogenic tank probe, and liquid N_2 was used as a cooling source. The temperature correction for –40 °C~–80 °C was calibrated by pure MeOH. The cooling power was set as 15~35% (15% at 0 °C and 35% at –80 °C). The UV-Vis spectra were recorded on a PerkinElmer Lambda 35 spectrophotometer and a Thermo Scientific Evolution 201 UV-Visible spectrophotometer.

2 Experimental Procedures

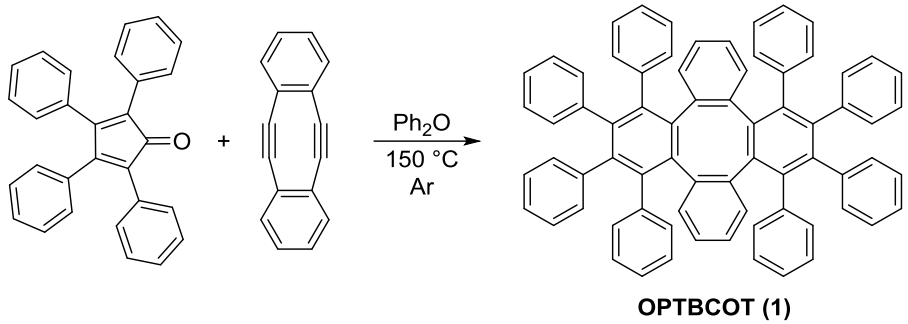

Scheme S1: Synthesis of **OPTBCOT (1)**.

9,14,23,28-Tetraphenyldiphenanthro[9,10-*b*:9',10'-*n*]tetraphenylene (OPTBCOT, 1). A Schlenk tube was charged with 2,3,4,5-tetraphenyl-2,4-cyclopentadien-1-one (379 mg, 986 µmol) and 5,6,11,12-tetradehydrodibenzo[*a*,*e*]cyclooctene (65.7 mg, 328 µmol). Both compounds were dissolved in Ph_2O (7.50 mL) under argon atmosphere and the solution was stirred at 150°C for 51h. Additional 2,3,4,5-tetraphenyl-2,4-cyclopentadien-1-one (126 mg, 329 µmol) was added and the mixture stirred further 1.5 h at 150°C. The reaction was cooled to rt and the solvent evaporated via vacuum distillation (91.0°C, 1.4×10^{-1} mbar). Recrystallization of the crude material from CH_2Cl_2/MeOH afforded **1** (189 mg, 207 µmol) as colorless crystals in 63% yield.

M.p.: >400°C.

R_f = 0.74 (SiO_2, hexanes/CH_2Cl_2 1:1).

^{1}H NMR (400 MHz, $CDCl_3$): δ = 7.08 (d, J = 7.7 Hz, 4H), 6.96 (td, J = 7.6, 1.4 Hz, 4H), 6.90–6.78 (m, 20H), 6.77–6.69 (m, 8H), 6.66–6.62 (m, 4H), 6.56 (td, J = 7.6, 1.4 Hz, 4H), 5.89 (d, J = 7.8 Hz, 4H) ppm.

^{13}C NMR (150 MHz, $CDCl_3$): δ = 141.2, 140.7, 140.7, 140.5, 139.8, 138.4, 138.0, 132.6, 132.5, 131.9, 131.8, 130.8, 129.2, 128.4, 126.9, 126.7, 126.6, 126.4, 125.5, 125.5, 125.2, 125.1 ppm.

HRMS (MALDI, dctb): calcd. for $C_{72}H_{48}$: 912.3751 [M^+]; found: 912.3746.

Crystallization of $C_{72}H_{48}$·THF (1-THF)

3 mg of **1** was dissolved in THF (2 mL), the solution filtered into an L-shaped glass ampule (*ca*. 18 cm length, O.D. 1 cm) which was sealed under reduced pressure. The ampule was placed over a sand bath (130 °C) for slow solvent evaporation. Colorless plate-shaped crystals deposited along the walls of the ampule after 5 days. Yield: 2.8 mg, 93%.

Crystallization of $C_{72}H_{48}$ (1-NS)

5 mg of **1** was sealed in a glass ampule (*ca*. 8 cm length, O.D. 1 cm) under vacuum, and the ampule was placed into an electric oven having a small temperature gradient along the length of the tube. The temperature was set at 300 °C. Colorless block-shaped crystals deposited in the cold zone after 7 days. Yield: 4.2 mg, 84%.

Preparation of $[\{Li^+(THF)_4\}_2\{Li^+_2(1^{4-})\}]$·2THF (2·2THF)

THF (2.0 mL) was added to a customized glass system containing excess Li metal (1.5 mg, 0.214 mmol) and **1** (2 mg, 0.0022 mmol, sublimed). The mixture was allowed to stir under argon at 25 ˚C for 24 h in a closed system. The initial color of the suspension was colorless (neutral ligand), and it changed to pale blue after 3.5 hours, purple after 4 hours, black-brown after 10 hours, and remained the same color until the reaction was stopped. The suspension was filtered, and the black-brown filtrate was layered with 1.5 mL of hexanes and placed at 5 ˚C. Dark brown plate-shaped crystals were present in good yield after 5 days. Yield: 2.7 mg, 75%. UV-Vis (THF, nm): λ_{max} 356, 459, 573. ^{1}H NMR (THF-d_8, ppm, –80 ˚C): δ = 4.26–4.28 (2H), 4.51–4.53 (2H), 4.82–4.84 (2H), 5.43–5.46 (2H), 5.72–5.74 (4H), 6.00–6.39 (18H), 6.52–6.87 (10H), 6.98–7.13 (6H), 7.24–7.26 (2H). ^{7}Li NMR (THF-d_8, ppm, –80 ˚C): δ = –5.08 (1Li), –1.88 (1Li), –0.55 (2Li).

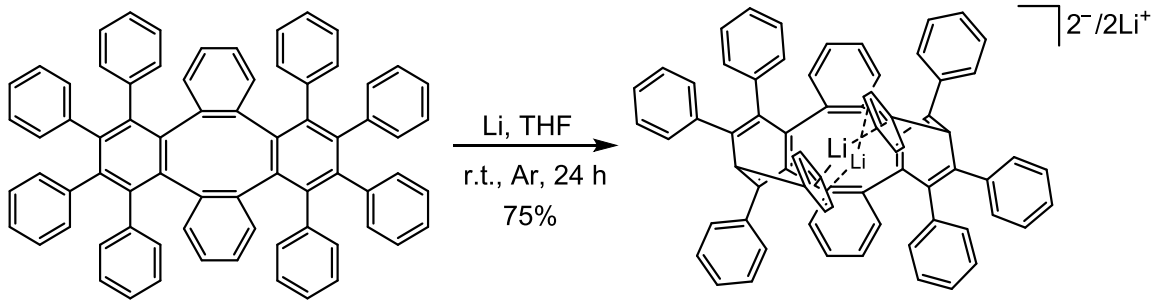

Scheme S2. Chemical reduction of **1**.

3 UV-Vis Spectroscopic Study

Sample preparation: Lithium (0.2 mg, 0.029 mmol) and **1** (0.5 mg, 0.0005 mmol, sublimed) were added into a small storage ampule (6.0 mL) with a Teflon stopper in the glove box, followed by the addition of anhydrous THF (2 mL). The UV-Vis spectra of the mixture (0.27 mM in THF) were monitored at different reaction times at room temperature.

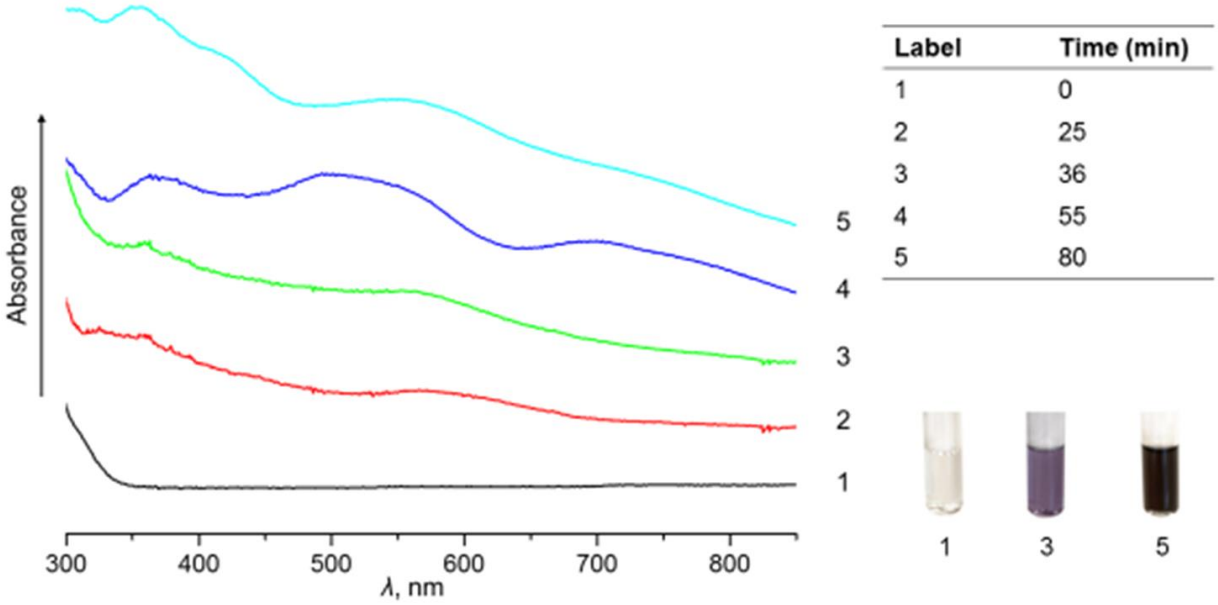

Figure S1. UV-Vis spectra of Li/**1** in THF.

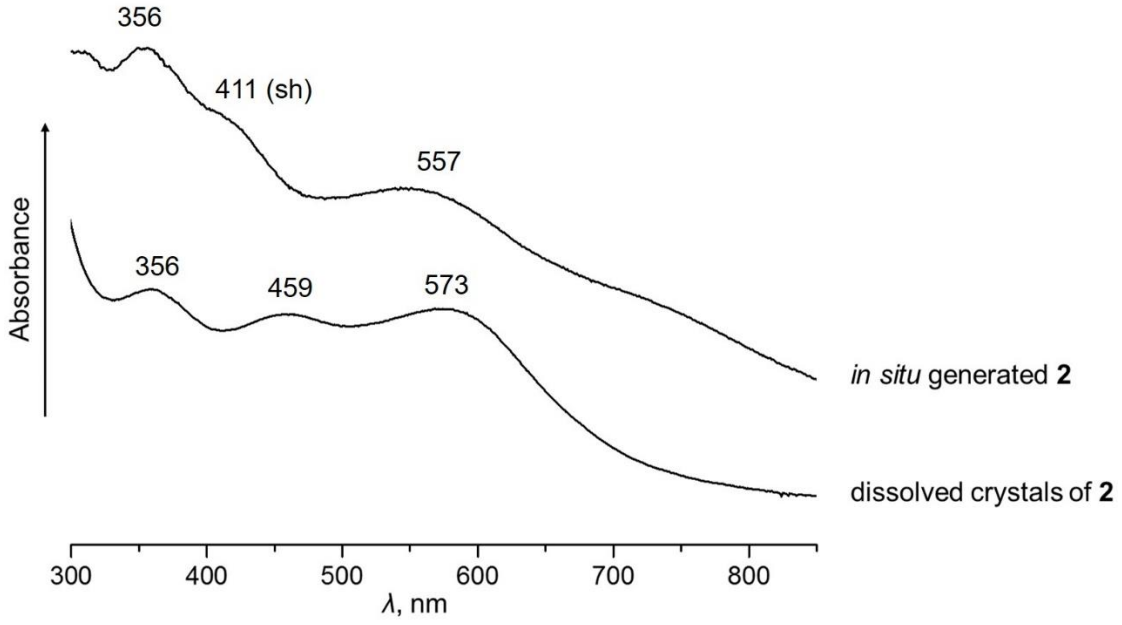

Figure S2. UV-Vis spectra of *in situ* generated **2** and crystals of **2**·2THF dissolved in THF.

4 NMR Spectroscopic Investigation

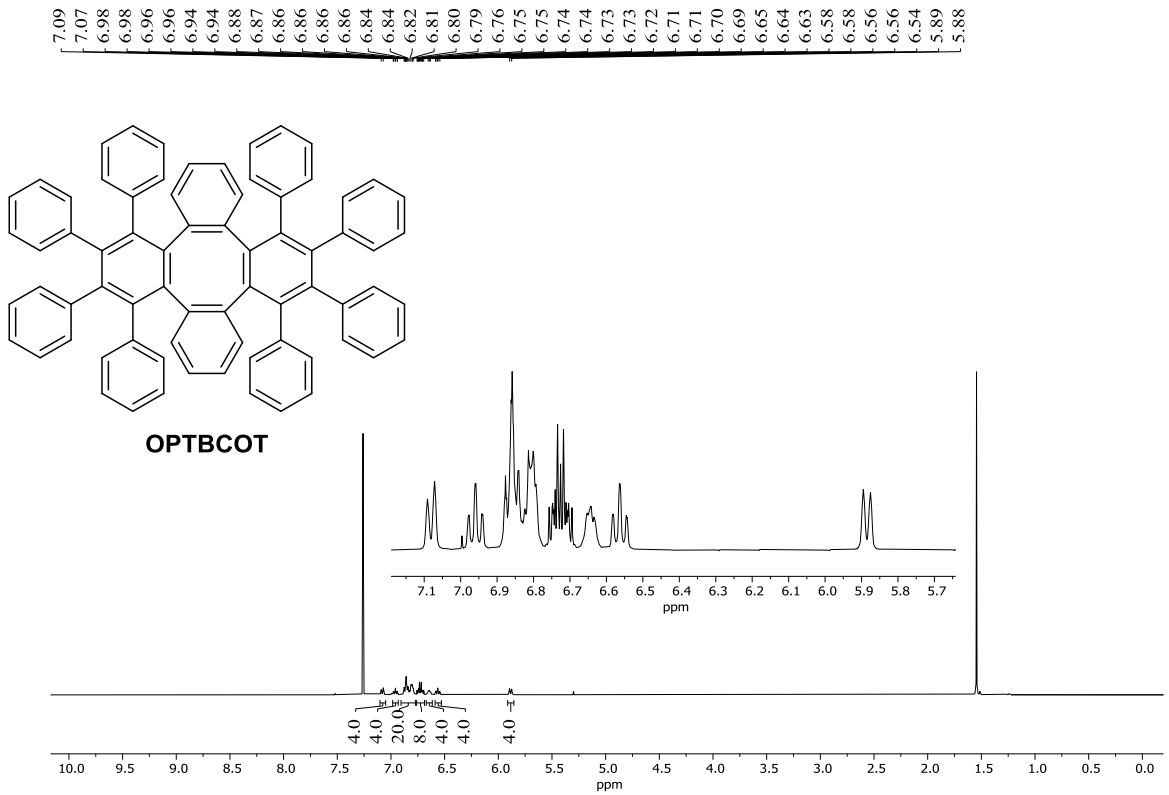

Figure S3. ^{1}H NMR spectrum of **1** ($CDCl_3$, 400 MHz).

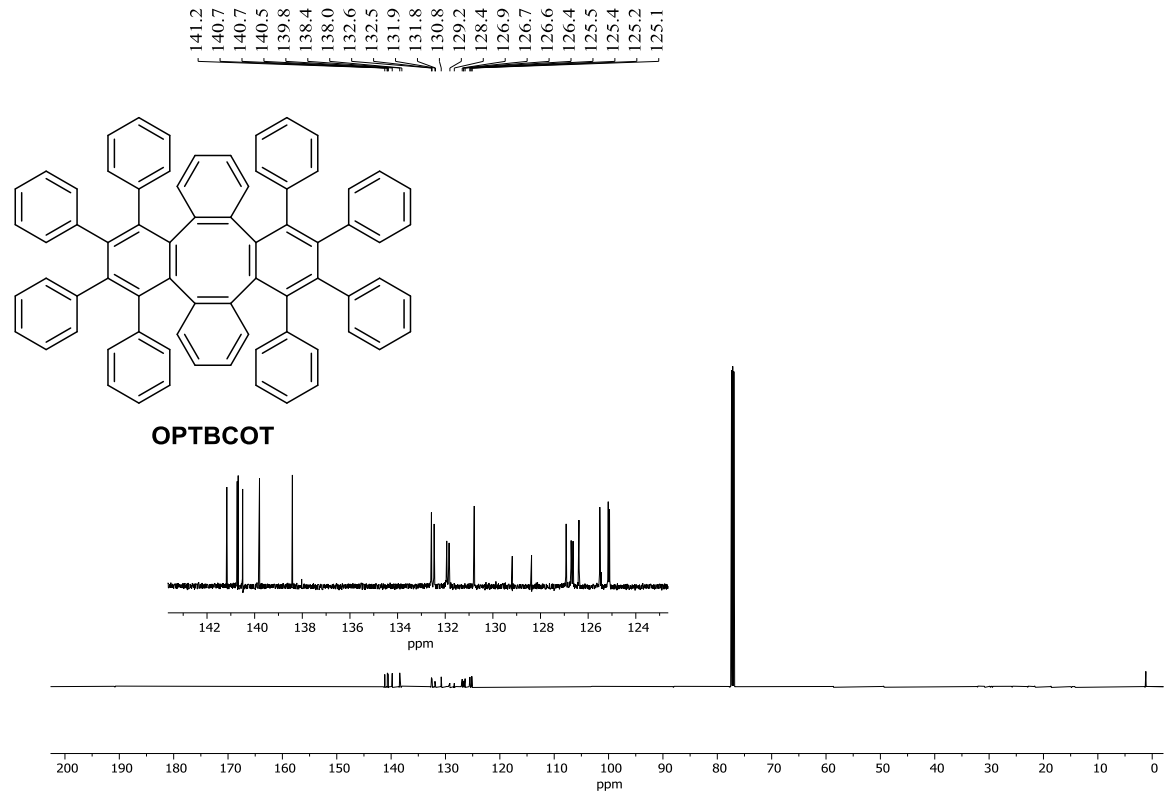

Figure S4. ^{13}C NMR spectrum of **1** ($CDCl_3$, 150 MHz).

Sample preparation: Crystals of **2**·2THF (5 mg) were washed with anhydrous hexanes and dried *in-vacuo*. Crystals were added into an NMR ampule (O.D. 5 mm) in the glove box, followed by the addition of anhydrous THF-d_8 (0.6 mL) to afford a dark brown solution. The NMR tube was sealed under argon.

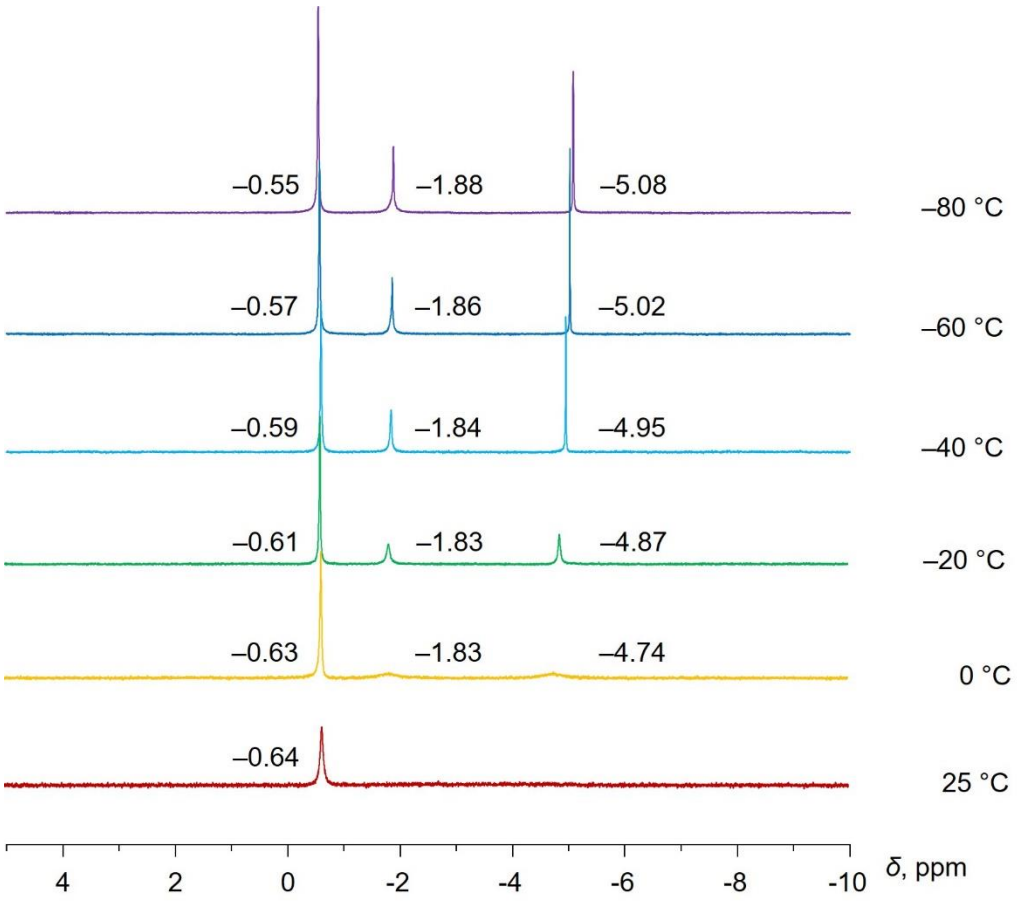

Figure S5. Variable-temperature ^{7}Li NMR spectra of **2** in THF-d_8 with chemical shifts.

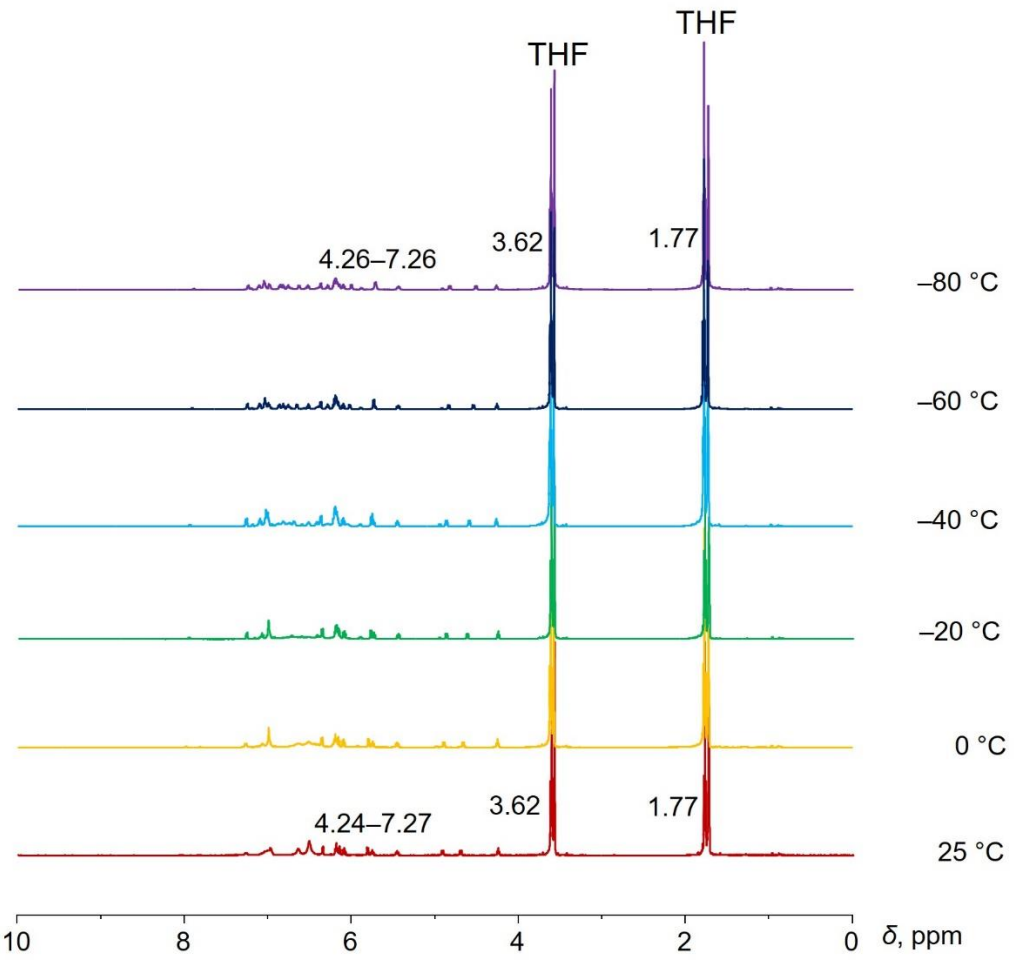

Figure S6. Variable-temperature ^{1}H NMR spectra of **2** in THF-d_8 with chemical shifts at 25 ºC and –80 ºC.

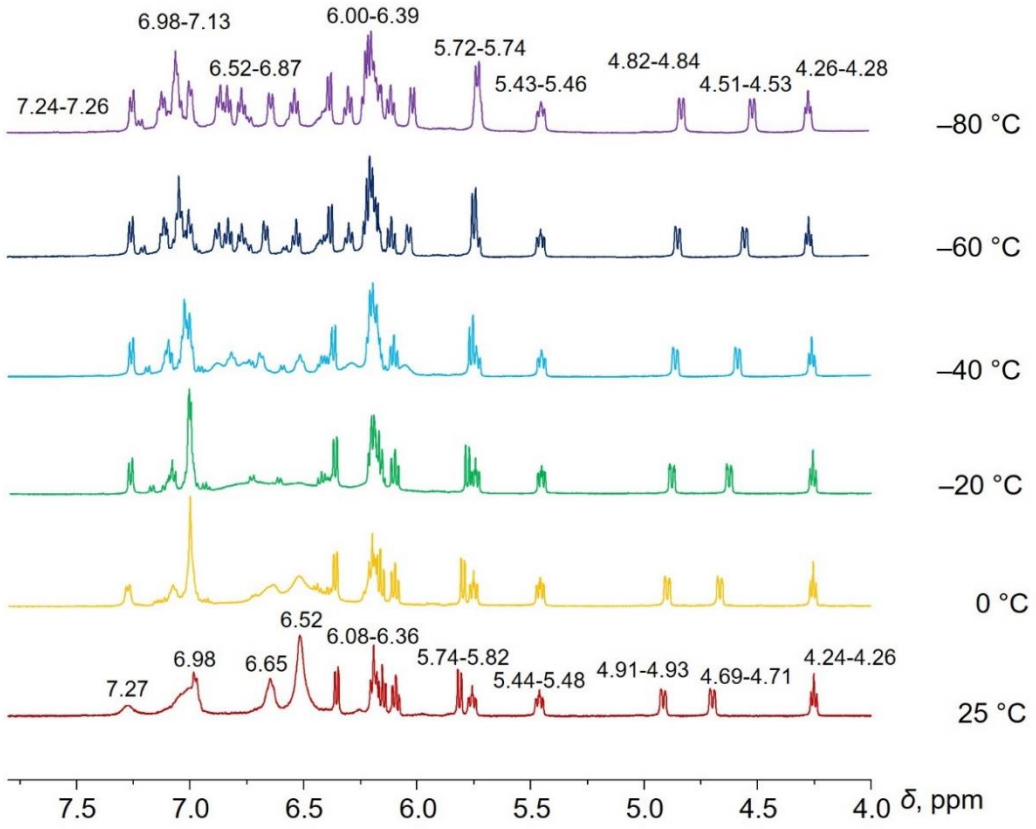

Figure S7. Variable-temperature ^{1}H NMR spectra of **2** in THF-d_8, aromatic region with chemical shifts at 25 ºC and –80 ºC.

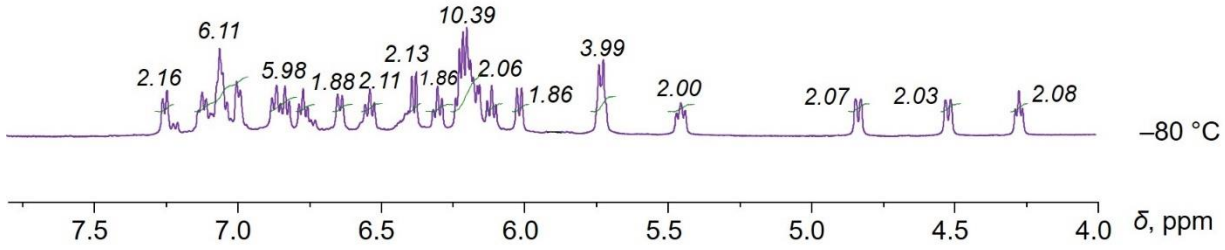

Figure S8. ^{1}H NMR spectrum of **2** in THF-d_8 at –80 ºC with integrations, aromatic region.

Redox Reversibility Study

Sample preparation: THF-d_8 (0.7 mL) was added to an NMR tube containing **1** (2 mg, 0.0022 mmol) and excess Li metal (1 mg, 0.143 mmol). The tube was sealed under argon. The ^{1}H NMR spectrum of **1** was collected immediately, and that of the *in situ* generated **2** was collected after 24 hours. The solution was then exposed to air by briefly opening the tube, and its spectrum was recorded as “quenched”.

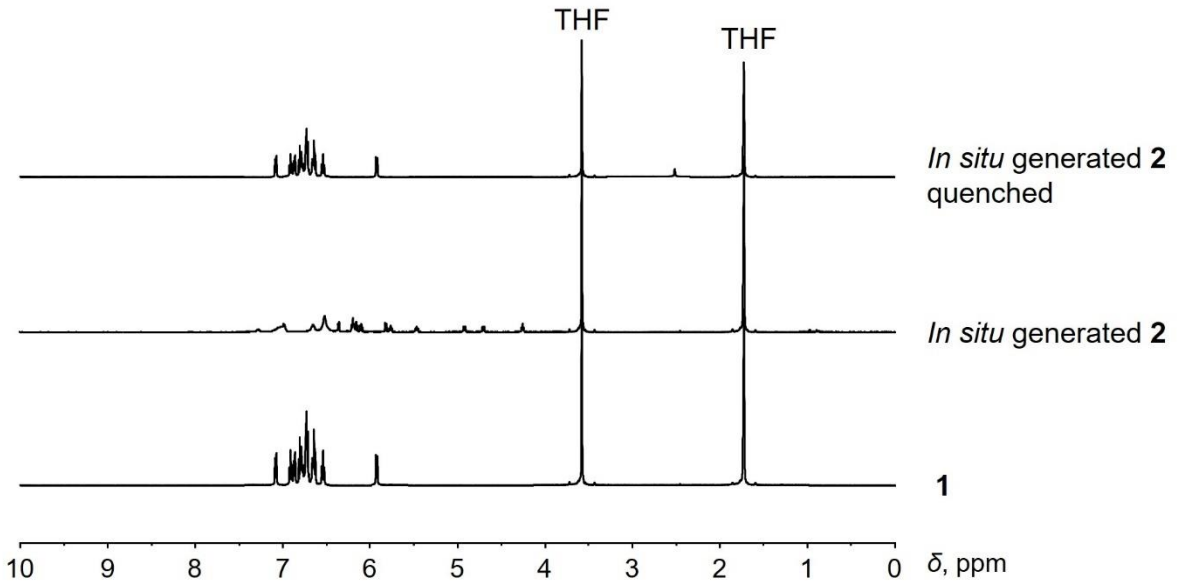

Figure S9. ^{1}H NMR spectra of **1**, *in situ* generated **2**, and its quenched product at 25 °C in THF-d_8.

5 Crystal Structure Solution and Refinement

Data collections of **1-NS** and **2**·2THF were performed on a Bruker VENTURE system equipped with a PHOTON 100 CMOS detector, a Cu-target INCOATEC IμS micro-focus X-ray source (λ = 1.54178 Å), and a mirror monochromator. Data were collected at 100(2) K crystal temperature (Oxford Cryosystems CRYOSTREAM 700), 50 kV and 1 mA for Cu radiation, with an appropriate 0.5° ω and φ scan strategy. Data collection of **1-THF** was performed at 100(2) K on a Bruker D8 fixed-χ system with a Pilatus1M CdTe pixel array detector using ϕ scans (synchrotron radiation at λ = 0.41328 Å) located at the Advanced Photon Source, Argonne National Laboratory (ChemMatCARS, Sector 15). Data reduction and integration were performed with SAINT (version 8.38A).[2] Data were corrected for absorption effects using the empirical methods as implemented in SADABS (version 2016/2).[3] The structures were solved by SHELXT (version 2018/2)[4] and refined by full-matrix least-squares procedures using the SHELXL program (version 2018/3)[5] through the OLEX2[6] graphical interface. All H-atoms were included at calculated positions and refined as riders, with U_{iso}(H) = 1.2 U_{eq}(C). In the asymmetric unit of **1-THF**, there is one independent OPTBCOT molecule and one THF molecule (Figure S11). The THF molecule and one phenyl ring of **1** were found to be disordered and modeled with two orientations. The geometries of the disordered parts were restrained to be similar. The anisotropic displacement parameters of the disordered molecules in the direction of the bonds were restrained to be equal with a standard uncertainty of 0.004 Å^2. They were also restrained to have the same U_{ij} components, with a standard uncertainty of 0.01 Å^2. In the asymmetric unit of **1-NS**, there are two independent OPTBCOT molecules (Figure S12). In the asymmetric unit of **2**·2THF, there are two independent [{$Li^+(THF)_4$}$_2${Li^+_2(**1**$^{4-}$)}] molecules (Figure S20), for which six coordinated THF molecules were found to be disordered and modeled with two orientations. The geometries of the disordered parts were restrained to be similar. The anisotropic displacement parameters of the disordered molecules in the direction of the bonds were restrained to be equal with a standard uncertainty of 0.004 Å^2. They were also restrained to have the same U_{ij} components, with a standard uncertainty of 0.01 Å^2. In the unit cell of **2**·2THF, eight interstitial THF molecules were found to be severely disordered and thus removed by the Olex2's solvent mask subroutine. The total void volume was 1328.8 Å^3, equivalent to 14.44% of the unit cell's total volume. Crystallographic data and details of the data collection and structure refinement are listed in Table S1.

Table S1. Crystallographic data of **1-THF**, **1-NS**, and **2**·2THF.

Compound	**1-THF**	**1-NS**	**2**·2THF
Empirical formula	$C_{76}H_{56}O$	$C_{72}H_{48}$	$C_{112}H_{128}Li_4O_{10}$
Formula weight	985.21	913.10	1661.90
Temperature (K)	100(2)	100(2)	100(2)
Wavelength (Å)	0.41328	1.54178	1.54178
Crystal system	Monoclinic	Triclinic	Monoclinic
Space group	$P2_1/n$	$P\bar{1}$	$P2_1$
a (Å)	11.7802(10)	11.7834(5)	14.1098(4)
b (Å)	38.390(4)	12.5520(5)	51.4140(13)
c (Å)	12.3459(13)	18.2032(7)	14.2813(4)
α (°)	90.00	82.9820(10)	90.00
β (°)	97.270(3)	72.7690(10)	117.3830(10)
γ (°)	90.00	82.4130(10)	90.00
V (Å^3)	5538.5(10)	2539.17(18)	9199.4(4)
Z	4	2	4
ρ_{calcd} (g·cm^{-3})	1.181	1.194	1.200
μ (mm^{-1})	0.032	0.512	0.575
F(000)	2080	960	3568
Crystal size (mm)	0.0052×0.0062×0.0098	0.09×0.19×0.23	0.03×0.10×0.17
θ range for data collection (°)	1.15-14.25	3.57-76.81	3.44-72.25
Reflections collected	40004	268523	142124
Independent reflections	9603 [R_{int} = 0.0946]	20481 [R_{int} = 0.0491]	34609 [R_{int} = 0.1033]
Transmission factors (min/max)	0.3976/0.4898	0.6046/0.7071	0.5158/0.5960
Data/restraints/params.	9603/945/805	20481/3/1297	34609/1403/2366
$R1$,[a] $wR2$[b] ($I > 2\sigma(I)$)	0.0856, 0.2203	0.0412, 0.1102	0.0571, 0.1244
$R1$,[a] $wR2$[b] (all data)	0.1103, 0.2407	0.0421, 0.1110	0.0832, 0.1391
Quality-of-fit[c]	1.080	1.043	1.041

[a] $R1 = \Sigma||F_o|-|F_c||/\Sigma|F_o|$. [b] $wR2 = [\Sigma[w(F_o^2-F_c^2)^2]/\Sigma[w(F_o^2)^2]]$.

[c] Quality-of-fit = $[\Sigma[w(F_o^2-F_c^2)^2]/(N_{obs}-N_{params})]^{½}$, based on all data.

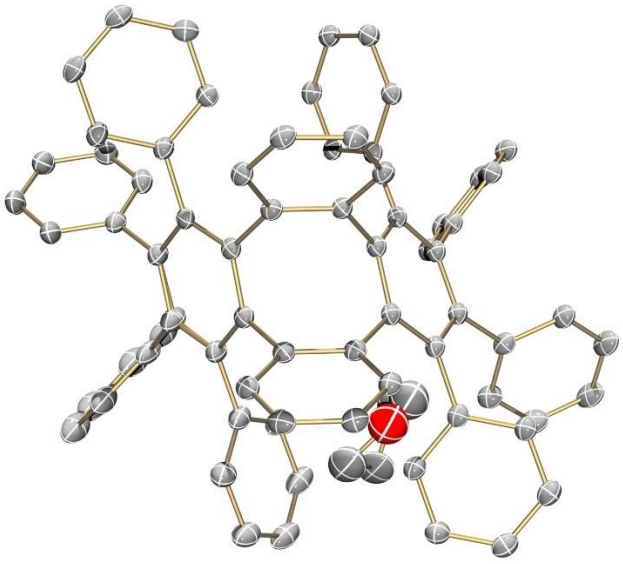

Figure S10. ORTEP drawing of the asymmetric unit of **1-THF** with thermal ellipsoids shown at the 40% probability level. Hydrogen atoms are omitted for clarity. The color scheme used: C grey, O red.

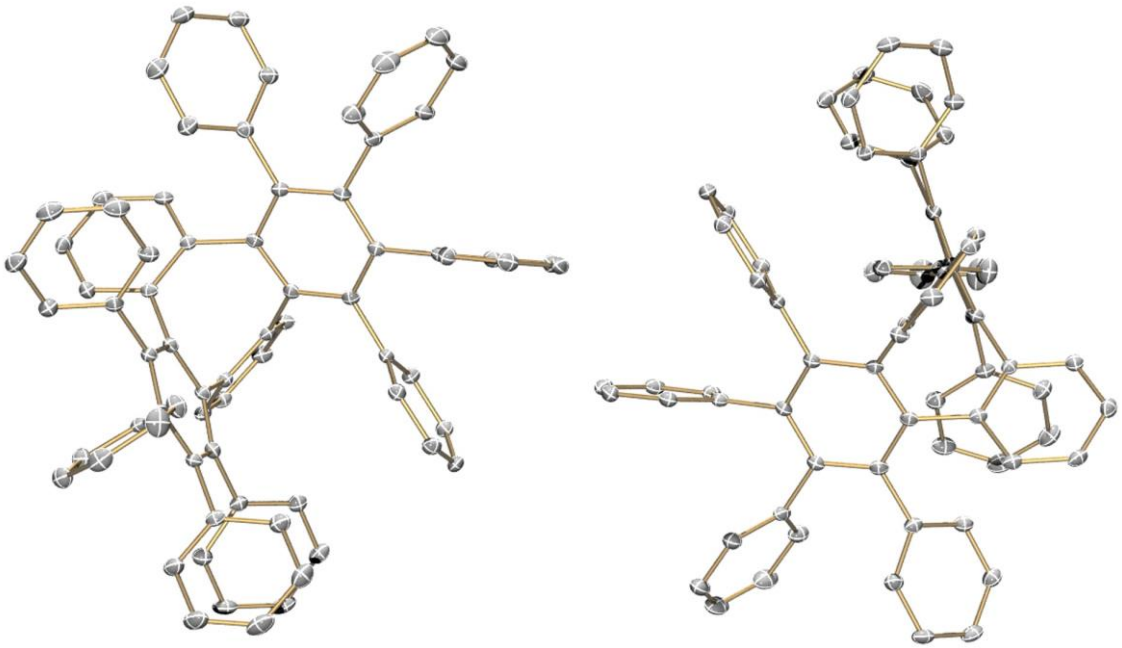

Figure S11. ORTEP drawing of the asymmetric unit of **1-NS** with thermal ellipsoids shown at the 40% probability level. Hydrogen atoms are omitted for clarity. There are two independent molecules in a unit cell. The color scheme used: C grey.

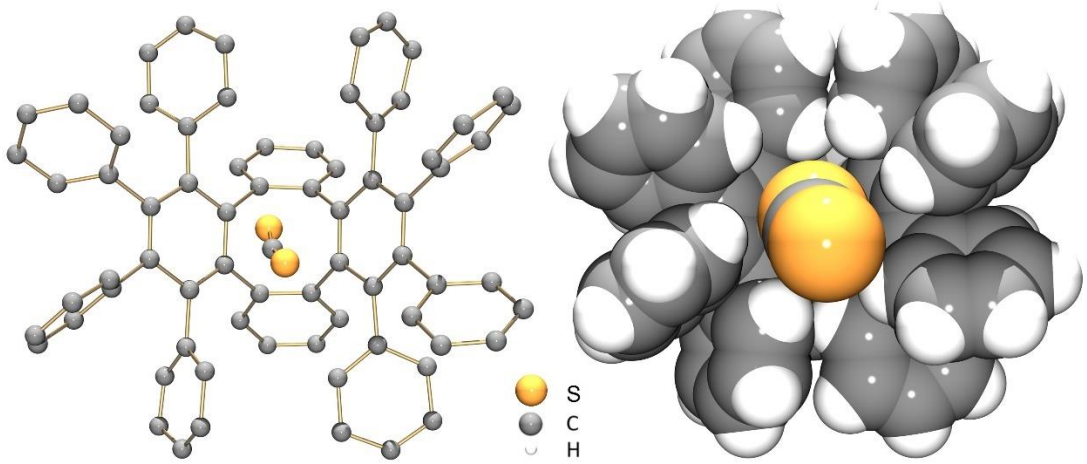

Figure S12. Crystal structure of the previously reported **1-CS_2**,[7] ball-and-stick (H-atoms are omitted) and space-filling models.

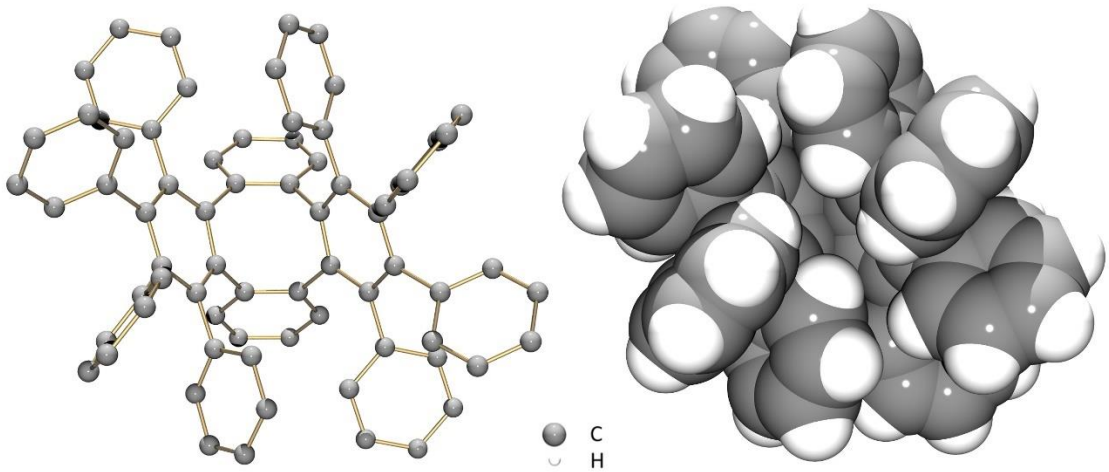

Figure S13. Crystal structure of **1-NS**, ball-and-stick (H-atoms are omitted) and space-filling models.

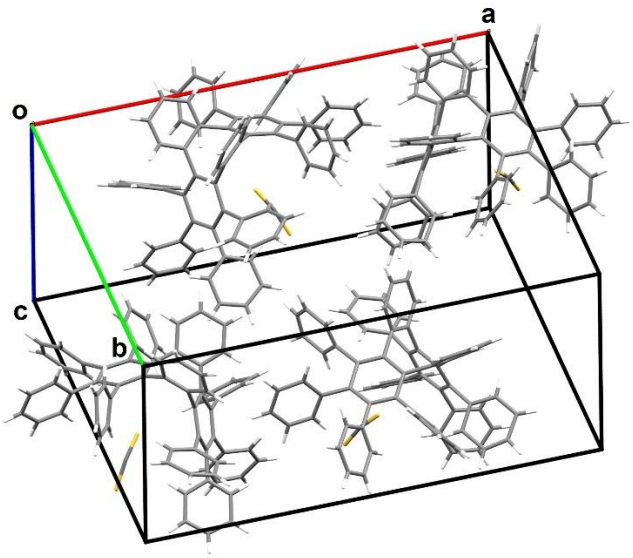

Figure S14. The unit cell of **1-CS_2**,[7] capped-stick model.

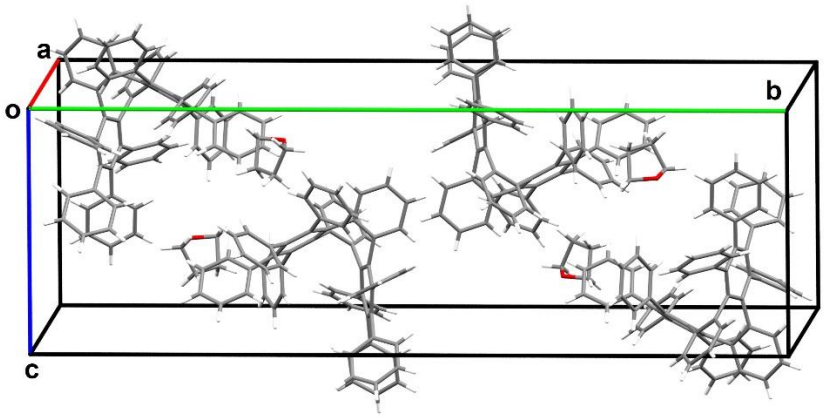

Figure S15. The unit cell of **1-THF**, capped-stick model.

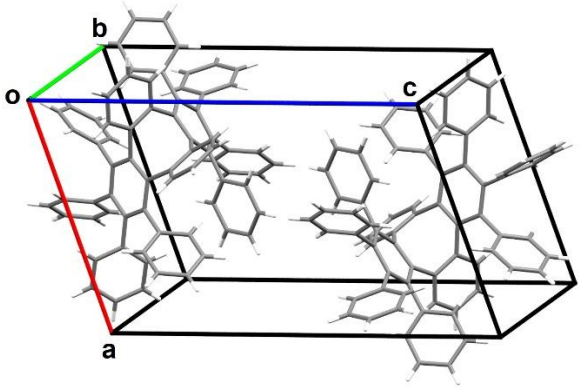

Figure S16. The unit cell of **1-NS**, capped-stick model.

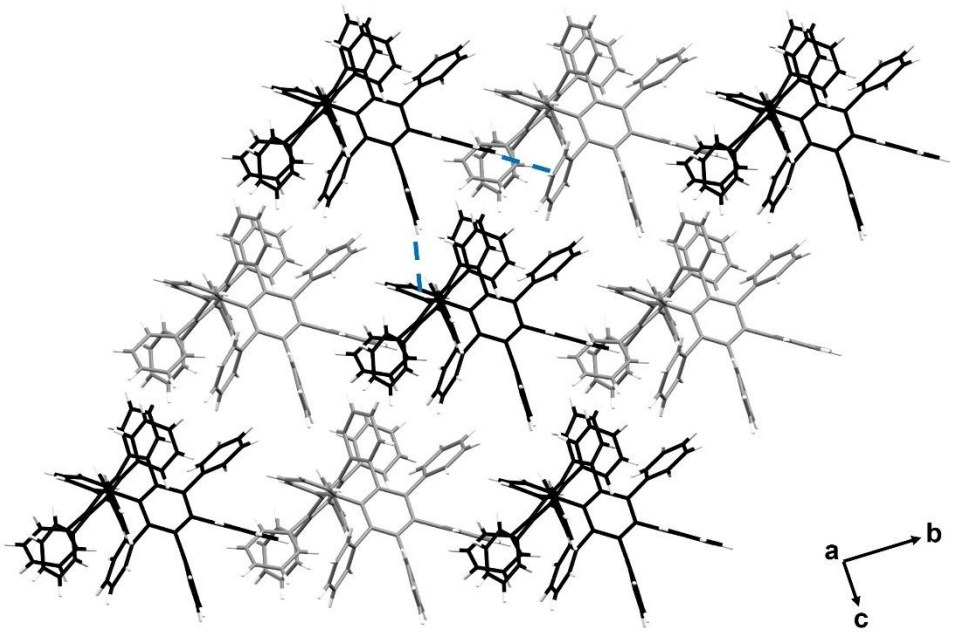

Figure S17. Solid-state structure of **1-CS$_2$**,[7] capped-stick model. Two conformations are shown in gray and black. The CS_2 molecules are omitted for clarity. C–H···π interactions are shown in blue.

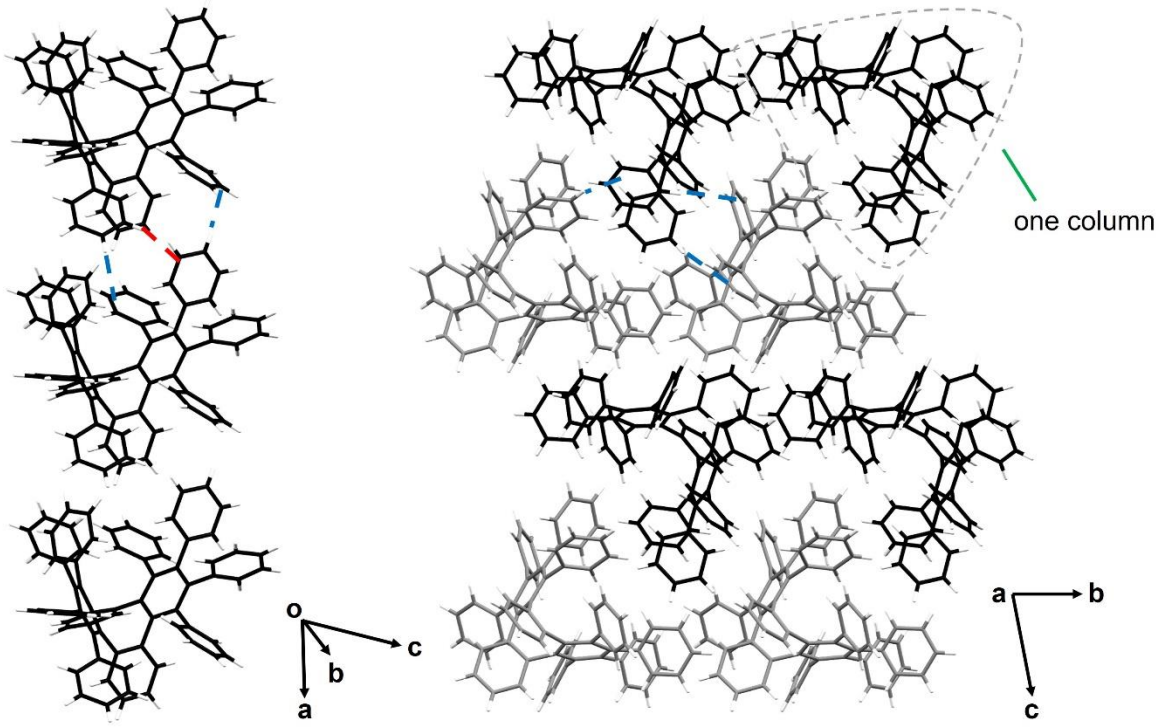

Figure S18. Solid-state structure of **1-NS**, capped-stick model. Two conformations are shown in gray and black. C–H···π and π···π interactions are shown in blue and red.

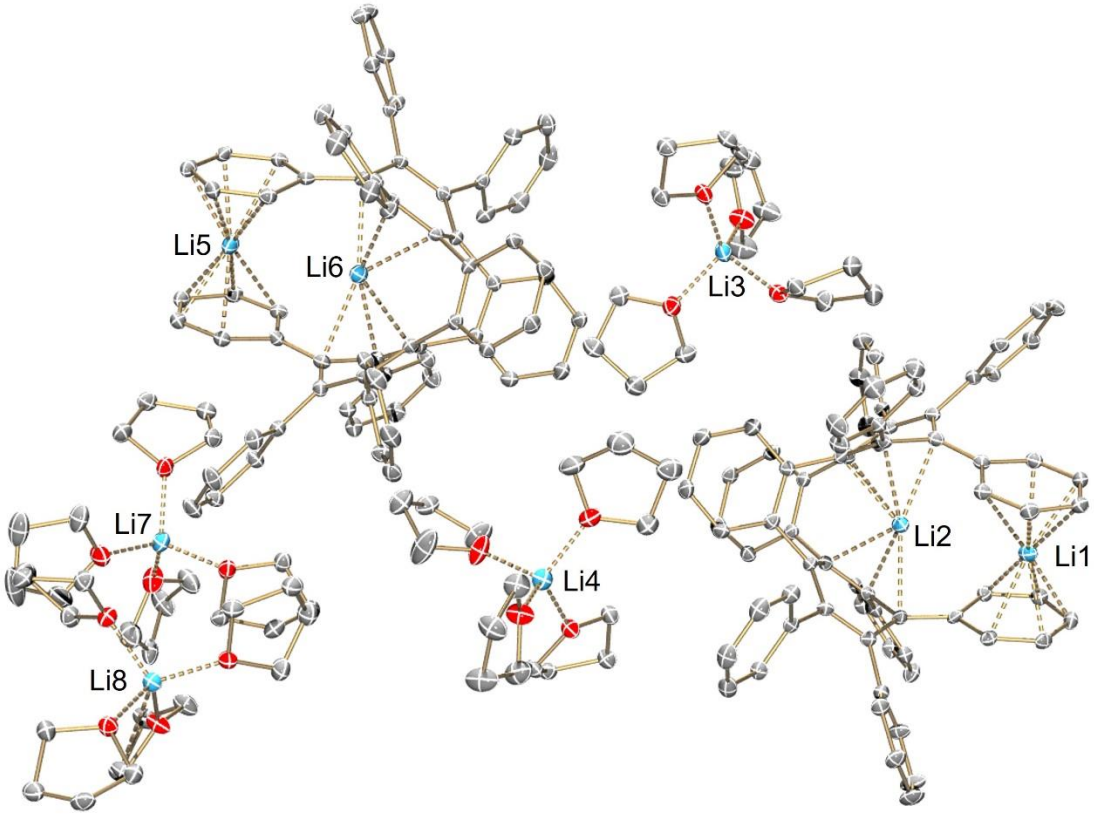

Figure S19. ORTEP drawing of the asymmetric unit of **2**·2THF with thermal ellipsoids shown at the 40% probability level. Hydrogen atoms and free THF molecules are omitted for clarity. There are two independent molecules in a unit cell. The color scheme used: C grey, O red, Li blue.

Table S2. Li–C bond length distances (Å) in **2**·2THF, along with the labeling scheme.

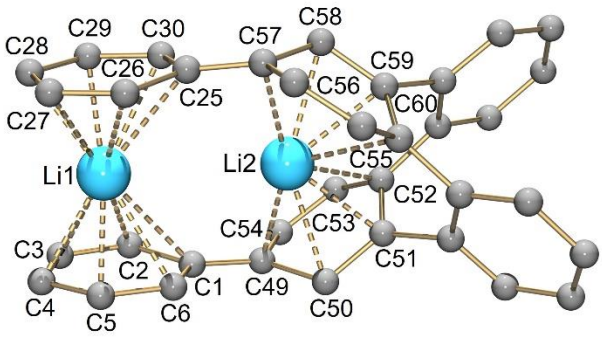

Bond	Distance	Bond	Distance	Bond	Distance	Bond	Distance
Li1–C1	2.584(9)	Li2–C49	2.370(8)	Li5–C73	2.593(9)	Li6–C121	2.372(9)
Li1–C2	2.379(9)	Li2–C50	2.343(9)	Li5–C74	2.395(9)	Li6–C122	2.353(9)
Li1–C3	2.261(9)	Li2–C51	2.303(9)	Li5–C75	2.271(9)	Li6–C123	2.318(9)
Li1–C4	2.268(9)	Li2–C52	2.544(9)	Li5–C76	2.273(9)	Li6–C124	2.552(9)
Li1–C5	2.304(9)	Li2–C53	3.149(9)	Li5–C77	2.299(9)	Li6–C125	3.131(9)
Li1–C6	2.436(9)	Li2–C54	3.150(9)	Li5–C78	2.425(9)	Li6–C126	3.135(9)
Li1–C25	2.575(9)	Li2–C55	3.095(9)	Li5–C97	2.640(9)	Li6–C127	3.195(9)
Li1–C26	2.379(9)	Li2–C56	3.111(9)	Li5–C98	2.465(9)	Li6–C128	3.156(9)
Li1–C27	2.268(9)	Li2–C57	2.385(9)	Li5–C99	2.312(9)	Li6–C129	2.354(9)
Li1–C28	2.267(9)	Li2–C58	2.382(8)	Li5–C100	2.238(9)	Li6–C130	2.318(9)
Li1–C29	2.296(9)	Li2–C59	2.305(8)	Li5–C101	2.255(9)	Li6–C131	2.310(9)
Li1–C30	2.420(9)	Li2–C60	2.524(9)	Li5–C102	2.419(9)	Li6–C132	2.600(9)

Table S3. Selected dihedral angles (°) in **1-CS$_2$**[7], **1-THF**, **1-NS**, and **1**$^{4-}$ (in **2**·2THF), along with the labeling schemes.

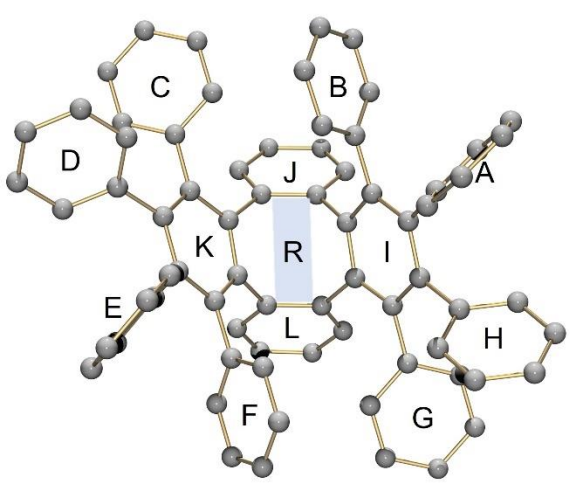

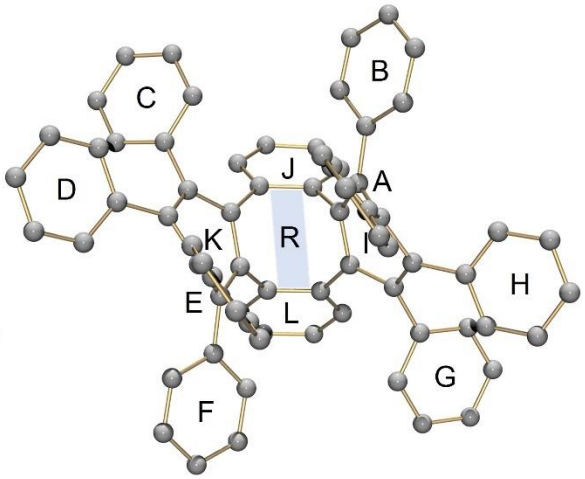

Dihedral Angle	**1-CS$_2$**[7]	**1-THF**	**1-NS**		**1**$^{4-}$	
			core 1	core 2	core 1	core 2
A/R	81.5	86.9	87.7	84.4	85.9	89.6
B/R	56.7	54.2	59.0	50.7	48.5	39.5
C/R	26.8	13.1	14.5	10.5	28.0	23.3
D/R	41.2	38.9	53.4	40.6	33.6	30.5
E/R	89.1	89.3	74.0	88.0	88.9	86.3
F/R	57.7	57.4	31.6	57.3	37.7	47.3
G/R	13.8	13.6	14.1	16.3	23.7	33.5
H/R	48.9	47.3	40.4	49.8	31.2	30.7
I/R	47.9	54.7	52.2	57.1	62.2	61.2
J/R	56.2	56.7	59.3	67.2	61.8	59.5
K/R	40.8	54.7	48.9	55.9	60.7	62.9
L/R	56.6	59.5	56.8	59.5	59.1	59.9

Table S4. Selected torsion angles of the eight-membered ring (°) in **1-CS$_2$**[7], **1-THF**, **1-NS**, and **1**$^{4-}$ (in **2**·2THF), along with the labeling schemes.

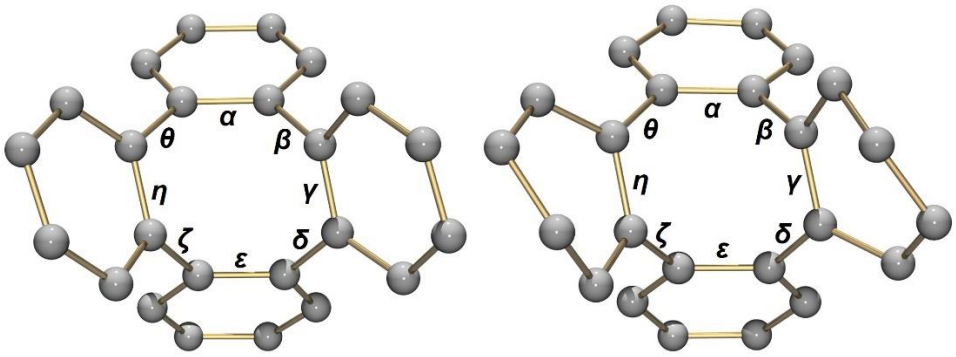

Torsion Angle	**1-CS$_2$**[7]	**1-THF**	**1-NS**		**1**$^{4-}$	
			core 1	core 2	core 1	core 2
α	1.1	2.9	3.4	2.4	4.9	2.0
β	71.9	81.2	61.6	83.5	60.0	58.2
γ	1.4	15.5	12.7	16.6	13.4	18.4
δ	72.2	60.3	76.2	58.3	87.3	90.4
ε	7.7	2.9	4.8	1.1	4.2	4.2
ζ	66.5	82.9	56.6	85.5	58.6	59.2
η	5.0	17.7	17.9	18.4	16.6	14.9
θ	64.0	58.3	81.6	57.7	90.5	86.4

Table S5. Planarity calculations (°) of rings I and K in **1-THF**, **1-NS**, and $\mathbf{1}^{4-}$ (in **2**·2THF).

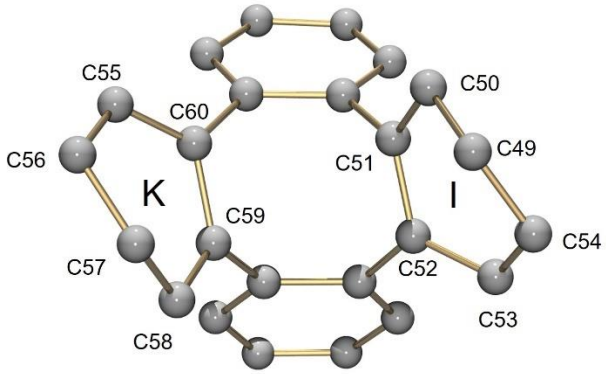

		1-THF	**1-NS**		$\mathbf{1}^{4-}$	
			core 1	core 2	core 1	core 2
Ring I	C49	–0.043	–0.049	0.042	–0.287	–0.277
	C50	–0.007	0.029	0.003	0.172	0.168
	C51	0.054	–0.018	–0.051	0.073	0.069
	C52	–0.052	–0.004	0.053	–0.204	–0.195
	C53	0.003	0.015	–0.008	0.093	0.086
	C54	0.044	–0.005	–0.039	0.153	0.149
		0.324x+0.946y–0.014z+22.922=0 (RMAS/A: 0.040)	0.324x+0.888y+0.328z+19.687=0 (RMAS/A: 0.017)	–0.327x–0.004y+0.945z+3.838=0 (RMAS/A: 0.038)	0.692x–0.551y+0.466z–7.930=0 (RMAS/A: 0.178)	0.386x+0.194y+0.902z+8.456=0 (RMAS/A: 0.172)
Ring K	C55	0.006	0.004	0.001	–0.087	–0.093
	C56	0.029	0.042	0.035	–0.144	–0.155
	C57	–0.040	–0.038	–0.026	0.274	0.284
	C58	0.016	–0.011	–0.018	–0.172	–0.174
	C59	0.019	0.058	0.054	–0.058	–0.068
	C60	–0.030	–0.054	–0.045	0.188	0.202
		–0.301x+0.465y+0.832z+13.393=0 (RMAS/A: 0.026)	–0.338x–0.014y+0.941z+5.445=0 (RMAS/A: 0.040)	0.286x+0.807y+0.517z+4.448=0 (RMAS/A: 0.034)	0.330x+0.208y+0.921z+15.056=0 (RMAS/A: 0.169)	0.690x–0.568y+0.448z–10.668=0 (RMAS/A: 0.178)

Table S6. Selected bond length distances (Å) in **1-THF**, **1-NS**, and $\mathbf{1}^{4-}$ (in **2**·2THF).

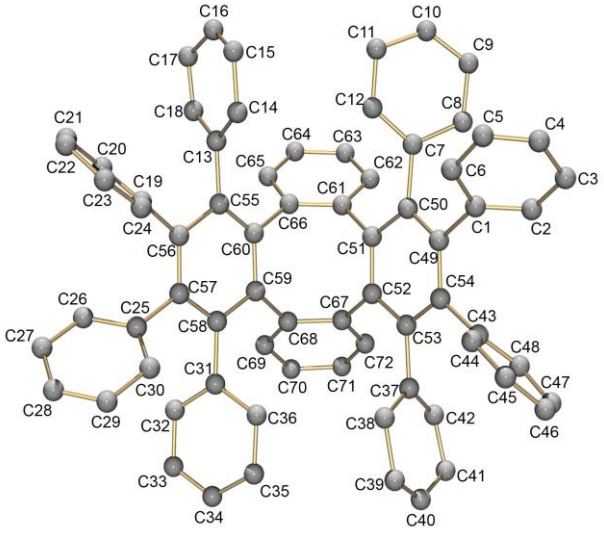

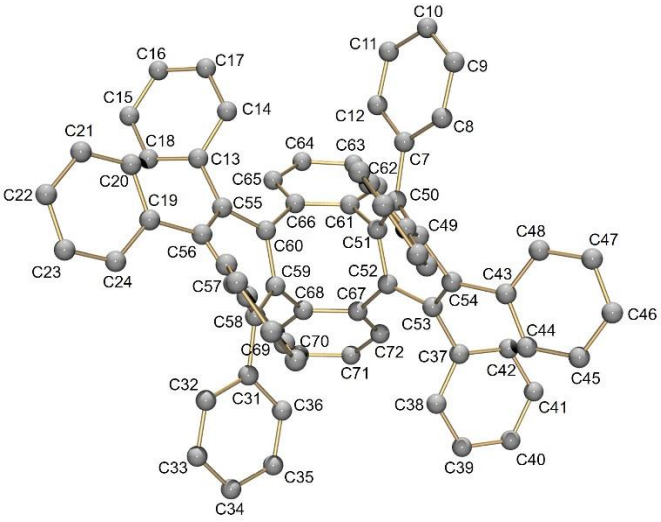

Bond	**1-THF**	**1-NS**	$\mathbf{1}^{4-}$	Bond	**1-THF**	**1-NS**	$\mathbf{1}^{4-}$
C1–C2	1.397(5)	1.385(4)	1.455(6)	C37–C38	1.402(5)	1.393(4)	1.400(6)
C1–C6	1.385(5)	1.397(4)	1.456(6)	C37–C42	1.396(5)	1.394(4)	1.390(6)
C1–C49	1.493(4)	1.501(4)	1.400(6)	C37–C53	1.495(5)	1.497(3)	1.491(6)
C2–C3	1.388(5)	1.391(4)	1.374(6)	C38–C39	1.388(5)	1.399(4)	1.384(7)
C3–C4	1.370(6)	1.376(5)	1.418(6)	C39–C40	1.387(5)	1.381(5)	1.390(8)
C4–C5	1.374(6)	1.388(5)	1.402(6)	C40–C41	1.394(5)	1.391(5)	1.397(7)
C5–C6	1.391(5)	1.387(4)	1.386(6)	C41–C42	1.388(5)	1.382(4)	1.397(6)
C7–C8	1.399(5)	1.400(4)	1.414(6)	C43–C44	1.400(5)	1.383(4)	1.396(6)
C7–C12	1.386(5)	1.396(4)	1.418(6)	C43–C48	1.384(5)	1.397(4)	1.409(6)
C7–C50	1.497(5)	1.499(4)	1.470(6)	C43–C54	1.498(4)	1.497(3)	1.478(6)
C8–C9	1.381(5)	1.390(4)	1.383(6)	C44–C45	1.382(5)	1.391(4)	1.403(6)
C9–C10	1.383(5)	1.394(5)	1.389(7)	C45–C46	1.384(5)	1.384(5)	1.392(7)
C10–C11	1.385(5)	1.383(5)	1.400(7)	C46–C47	1.387(5)	1.384(4)	1.369(7)
C11–C12	1.382(5)	1.391(4)	1.376(6)	C47–C48	1.394(5)	1.385(4)	1.387(6)
C13–C14	1.397(5)	1.400(4)	1.391(6)	C49–C50	1.405(5)	1.403(4)	1.495(6)
C13–C18	1.379(6)	1.399(4)	1.401(6)	C49–C54	1.410(5)	1.404(4)	1.484(6)
C13–C55	1.500(5)	1.496(4)	1.504(6)	C50–C51	1.407(4)	1.406(4)	1.403(6)
C14–C15	1.389(5)	1.386(4)	1.389(7)	C51–C52	1.410(5)	1.406(4)	1.428(6)
C15–C16	1.370(7)	1.388(4)	1.369(7)	C51–C61	1.486(4)	1.489(4)	1.500(6)
C16–C17	1.381(6)	1.385(4)	1.396(7)	C52–C53	1.395(4)	1.404(4)	1.447(6)
C17–C18	1.392(6)	1.391(4)	1.383(7)	C52–C67	1.513(4)	1.507(4)	1.497(6)
C19–C20	1.399(12)	1.396(4)	1.413(6)	C53–C54	1.406(4)	1.408(3)	1.378(6)

C19–C24	1.400(11)	1.390(4)	1.403(6)	C55–C56	1.416(9)	1.412(4)	1.370(6)
C19–C56	1.506(10)	1.495(4)	1.499(6)	C55–C60	1.399(5)	1.401(4)	1.440(6)
C20–C21	1.391(12)	1.394(4)	1.380(6)	C56–C57	1.408(9)	1.407(4)	1.499(6)
C21–C22	1.419(18)	1.382(5)	1.387(7)	C57–C58	1.405(5)	1.407(4)	1.492(6)
C22–C23	1.337(17)	1.381(5)	1.384(7)	C58–C59	1.394(5)	1.415(4)	1.394(6)
C23–C24	1.417(11)	1.394(4)	1.380(6)	C59–C60	1.406(5)	1.401(4)	1.451(6)
C25–C26	1.388(5)	1.395(4)	1.470(6)	C59–C68	1.489(4)	1.492(4)	1.490(6)
C25–C30	1.389(5)	1.388(4)	1.454(6)	C60–C66	1.506(5)	1.507(4)	1.494(6)
C25–C57	1.497(5)	1.503(4)	1.411(6)	C61–C62	1.398(5)	1.404(4)	1.382(6)
C26–C27	1.375(6)	1.392(5)	1.387(6)	C61–C66	1.407(5)	1.396(4)	1.419(6)
C27–C28	1.381(6)	1.371(6)	1.397(7)	C62–C63	1.378(5)	1.387(4)	1.380(6)
C28–C29	1.376(6)	1.383(6)	1.399(6)	C63–C64	1.390(5)	1.388(4)	1.394(6)
C29–C30	1.376(5)	1.400(5)	1.369(6)	C64–C65	1.381(5)	1.381(4)	1.384(6)
C31–C32	1.392(5)	1.398(4)	1.407(6)	C65–C66	1.399(5)	1.399(4)	1.403(6)
C31–C36	1.392(5)	1.395(4)	1.405(6)	C67–C68	1.401(4)	1.412(4)	1.406(6)
C31–C58	1.502(5)	1.501(4)	1.477(6)	C67–C72	1.390(5)	1.399(4)	1.393(6)
C32–C33	1.384(5)	1.386(4)	1.385(7)	C68–C69	1.397(4)	1.399(4)	1.395(6)
C33–C34	1.385(6)	1.387(5)	1.382(7)	C69–C70	1.380(5)	1.385(4)	1.390(7)
C34–C35	1.389(5)	1.384(5)	1.374(7)	C70–C71	1.383(5)	1.392(4)	1.375(7)
C35–C36	1.383(5)	1.392(4)	1.389(7)	C71–C72	1.386(5)	1.390(4)	1.400(6)

*Note: Only one core is shown for **1-NS** and **2**·2THF.*

6 Computational Details and Results

All the DFT calculations have been performed adopting the program package Turbomole (version 7.3).[8] The reported energies refer to structurally optimized molecules using the B3LYP density functional[9] and the def2-TZVP basis sets[10] from the Turbomole library. Van der Waals interactions were treated with Grimme's dispersion correction scheme D3,[11] and solvent effects were included within the conductor-like screening model (COSMO)[12] with ε_r = 7.6 mimicking THF. Throughout, the multipole accelerated RI method[13,14,15] was used to calculate the Coulomb part of the electronic energy.

Zero-point vibrational energies and thermal corrections to the free energy *G*° at standard conditions (T = 293.15 K, p = 1 bar) were calculated within the rigid rotator/harmonic oscillator approximations, whereby the contributions from low-frequency vibrations below 300 cm^{-1} were interpolated between a free rotator model and the (usual) harmonic oscillator model.[16] This methodology leads to a more balanced description of the entropy contributions from these low-frequency vibrations (within the commonly adopted harmonic approximation the entropy contributions of low-frequency vibrations are notoriously overestimated).

Nuclear independent chemical shifts (NICS)[17] were calculated using the TPSS density functional[18] and the def2-TZVP basis sets[10] from the Turbomole library. The implicit solvent model has been switched off in the NICS computations.

Coordination equilibria of $\mathbf{1}^{2-}$ As it is not a priori clear whether $\mathbf{1}^{2-}$ is coordinated by Li^+, we consider the energetics of the coordination reactions

$$\mathbf{1}^{2-} + [Li(THF)_4]^+ \rightarrow [Li^+(\mathbf{1}^{2-})]^- + 4\ THF$$

and

$$[Li^+(\mathbf{1}^{2-})]^- + [Li(THF)_4]^+ \rightarrow [Li^+_2(\mathbf{1}^{2-})] + 4\ THF$$

We find that the coordination of one Li+ cation by $\mathbf{1}^{2-}$ is strongly exergonic with $\Delta G° = -46.9$ kcal/mol (due to the large entropy gain in course of the reaction; the zero-point energy change is $\Delta E° = -6.3$ kcal/mol), whereas the second coordination is slightly endergonic by $\Delta G° = +3.0$ kcal/mol ($\Delta E° = +40.3$ kcal/mol). This suggests that the dianionic species is preferentially coordinated by one Li^+ cation in solution.

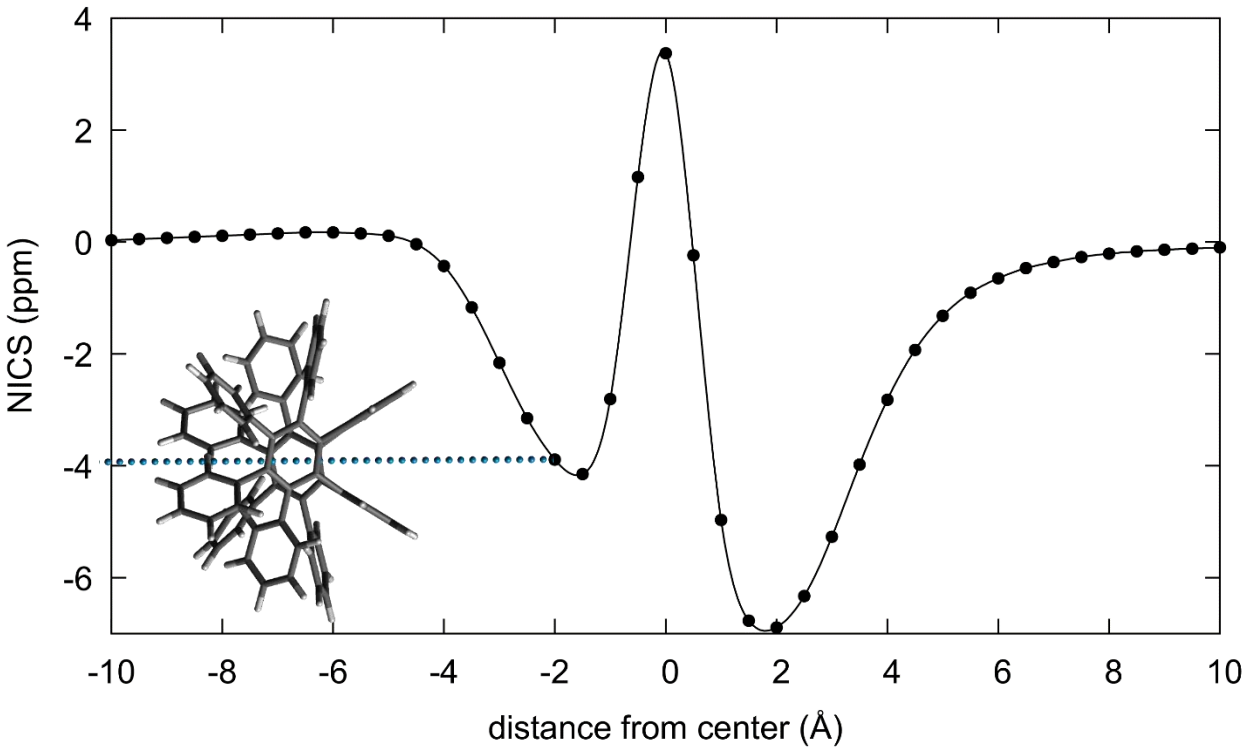

Figure S20. NICS scan of **1** through the geometrical center of the COT core. Molecular structure and NICS positions are depicted in the lower left corner.

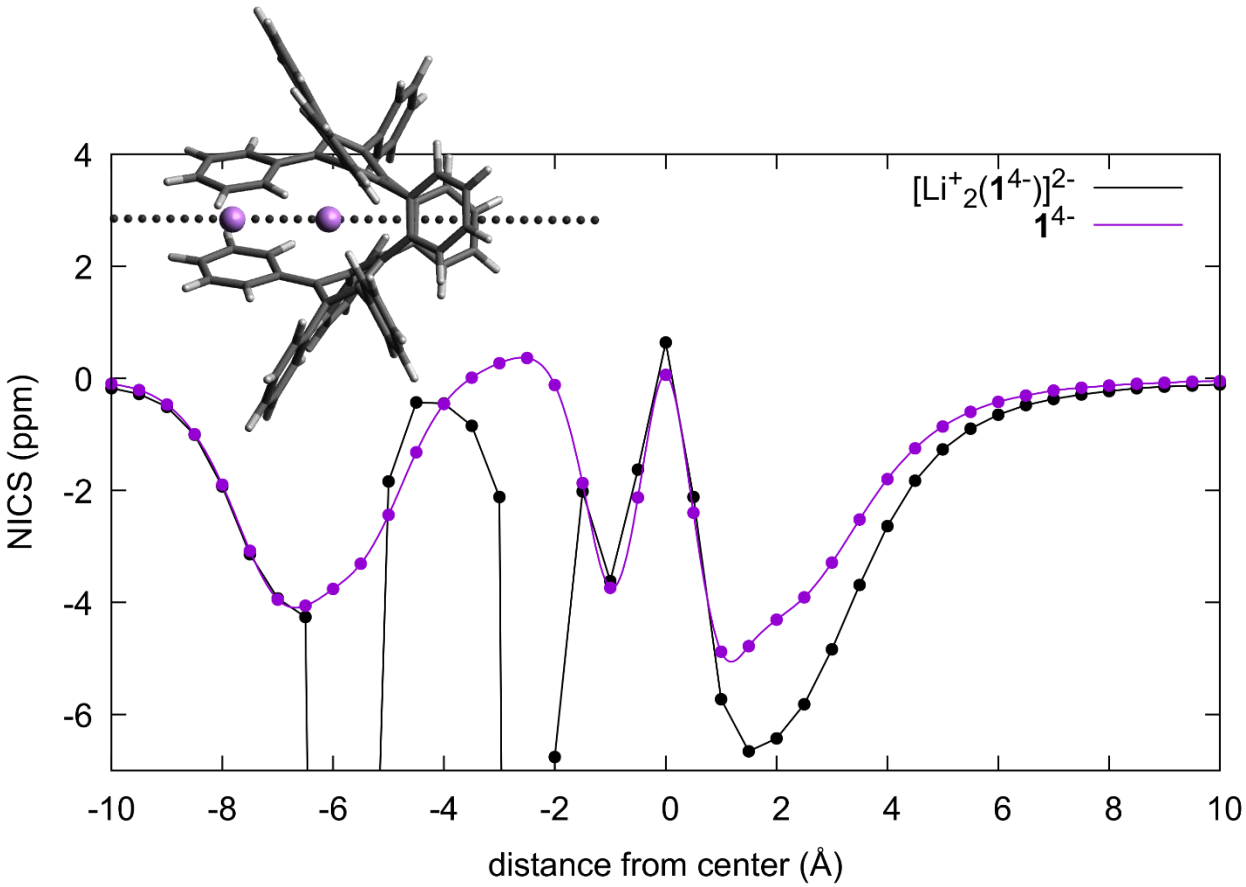

Figure S21. NICS scan of $[Li^{+}_{2}(\mathbf{1}^{4-})]^{2-}$ through the geometrical center of the COT core. Molecular structure and NICS positions are depicted in the upper left corner. Large negative NICS values occur near the Li^{+} cations. For comparison, the NICS scan of $\mathbf{1}^{4-}$ is shown as well indicating that the NICS values near the COT core are essentially unaffected by the Li^{+} cations.

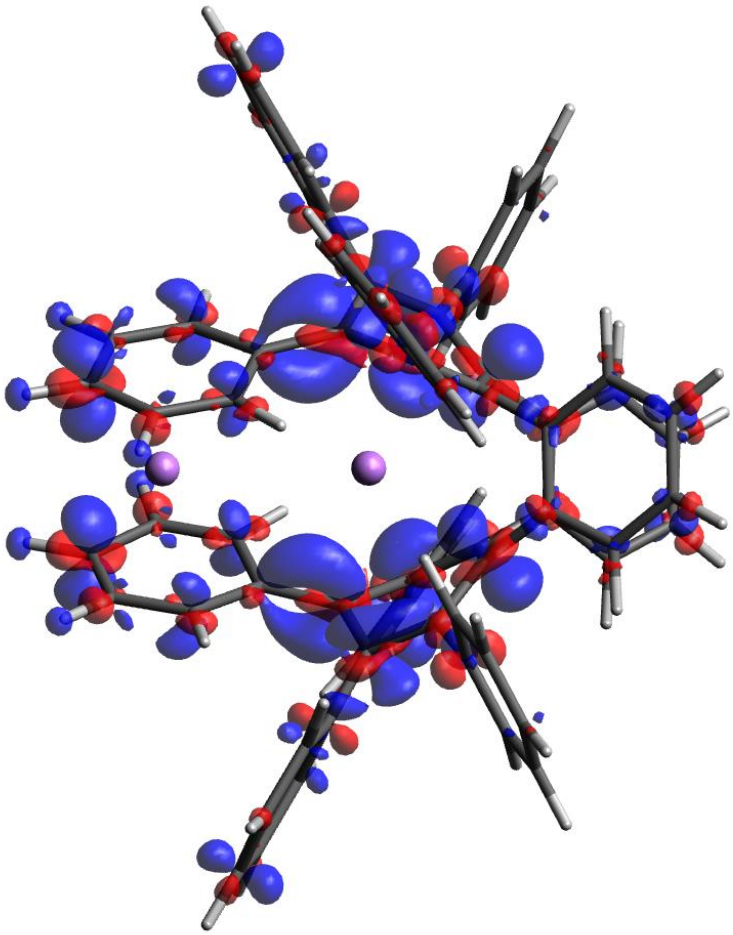

Figure S22. Charge density difference between $[Li^{+}_{2}(\mathbf{1}^{4-})]^{2-}$ and $[Li^{+}_{2}(\mathbf{1})]^{2+}$ (isovalue = 0.005 e/bohr^3); blue isosurfaces indicate an increase of the electron density, red isosurfaces a depletion of electron density.

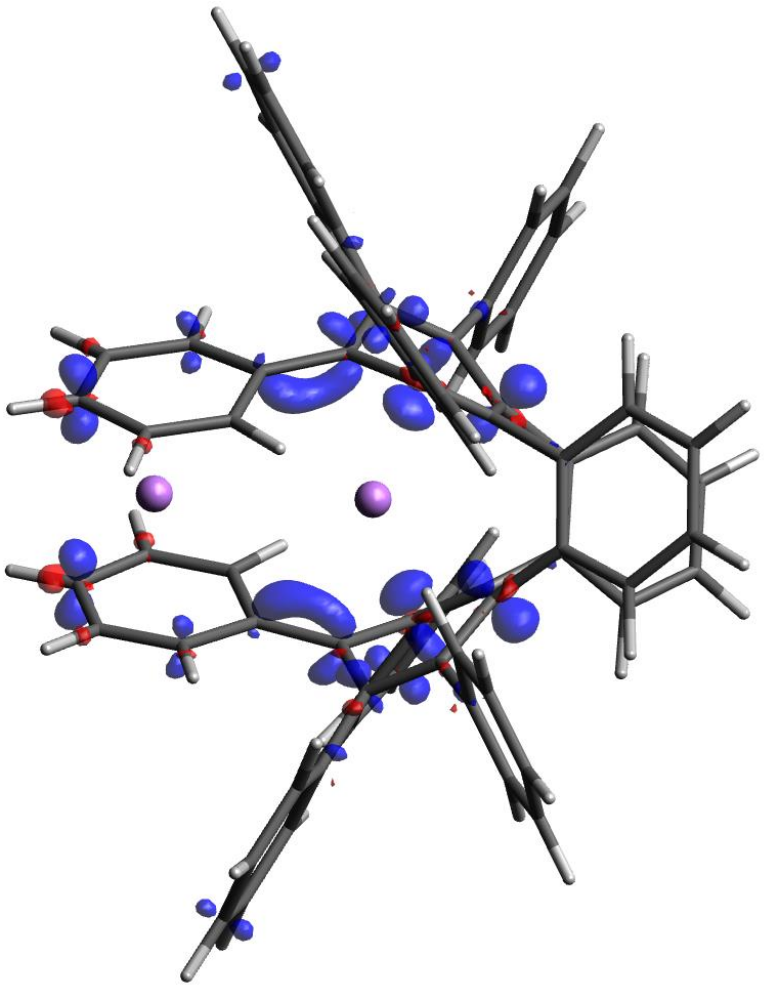

Figure S23. Charge density difference between $[Li^{+}_2(\mathbf{1}^{4-})]^{2-}$ and $[Li^{+}_2(\mathbf{1}^{2-})]$ (isovalue = 0.005 e/bohr^3); blue isosurfaces indicate an increase of the electron density, red isosurfaces a depletion of electron density.

	$[Li^{+}(\mathbf{1}^{2-})]^{-}$	$[Li^{+}_2(\mathbf{1}^{4-})]^{2-}$	$\mathbf{1}^{2-}$	$\mathbf{1}^{4-}$
COSMO(THF)	-2.42	-1.79	-0.71	-0.05
vacuum	-0.50	+1.73	+2.83	+6.66

Table S7. Calculated energies (in eV) of the highest occupied orbital (HOMO) of $\mathbf{1}^{2-}$ and $\mathbf{1}^{4-}$, both with/without coordinated Li cation(s) and with/without solvent effects.

7 References

[1] N. V. Kozhemyakina, J. Nuss, M. Jansen, *Z. Anorg. Allg. Chem.* **2009**, *635*, 1355-1361.

[2] SAINT; part of Bruker APEX3 software package (version 2017.3-0): Bruker AXS, **2017**.

[3] SADABS; part of Bruker APEX3 software package (version 2017.3-0): Bruker AXS, **2017**.

[4] G. M. Sheldrick, *Acta Crystallogr.* **2015**, *A71*, 3-8.

[5] G. M. Sheldrick, *Acta Crystallogr.* **2015**, *C71*, 3-8.

[6] O. V. Dolomanov, L. J. Bourhis, R. J. Gildea, J. A. K. Howard, H. Puschmann, *J. Appl. Crystallogr.* **2009**, *42*, 339-341.

[7] M. Müller, V. S. Iyer, C. Kübel, V. Enkelmann, K. Müllen, *Angew. Chem. Int. Ed. Engl.* **1997**, *36*, 1607-1610.

[8] TURBOMOLE V7.3 2018, a development of University of Karlsruhe and Forschungszentrum Karlsruhe GmbH, 1989-2007, TURBOMOLE GmbH, since 2007; available from *http://www.turbomole.com*.

[9] A. D. Becke, *J. Chem. Phys.* **1993**, *98*, 5648-5652.

[10] F. Weigend, R. Ahlrichs, *Phys. Chem. Chem. Phys.* **2005**, *7*, 3297-3305.

[11] S. Grimme, J. Antony, S. Ehrlich, H. Krieg, *J. Chem. Phys.* **2010**, *132*, 154104.

[12] A. Klamt, G. Schüürmann, *J. Chem. Soc., Perkin Trans. 2* **1993**, 799-805.

[13] K. Eichkorn, O. Treutler, H. Öhm, M. Häser, R. Ahlrichs, *Chem. Phys. Lett.* **1995**, *242*, 652-660.

[14] M. Sierka, A. Hogekamp, R. Ahlrichs, *J. Chem. Phys.* **2003**, *118*, 9136-9148.

[15] F. Weigend, *Phys. Chem. Chem. Phys.* **2006**, *8*, 1057-1065.

[16] S. Grimme, *Chem. Eur. J.* **2012**, *18*, 9955-9964.

[17] P. v. R. Schleyer, C. Maerker, A. Dransfeld, H. Jiao, N. J. R. van Eikema Hommes, *J. Am. Chem. Soc.* **1996**, *118*, 6317-6318.

[18] J. Tao, J. P. Perdew, V. N. Staroverov, G. E. Scuseria, *Phys. Rev. Lett.* **2003**, *91*, 146401.